Experimental and theoretical investigations of the He I 2 rovibronic spectra in the I 2 B – X , 20–0 region

Sara E. Ray, Anne B. McCoy, John J. Glennon, Joshua P. Darr, Elizabeth J. Fesser, Jeffrey R. Lancaster, and Richard A. Loomis

Citation: The Journal of Chemical Physics **125**, 164314 (2006); doi: 10.1063/1.2363378
View online: http://dx.doi.org/10.1063/1.2363378
View Table of Contents: http://scitation.aip.org/content/aip/journal/jcp/125/16?ver=pdfcov
Published by the AIP Publishing

Experimental and theoretical investigations of the He···I_2 rovibronic spectra in the I_2 *B*–*X*, 20–0 region

Sara E. Ray and Anne B. McCoy[a)]
Department of Chemistry, The Ohio State University, Columbus, Ohio 43210

John J. Glennon, Joshua P. Darr, Elizabeth J. Fesser,
Jeffrey R. Lancaster, and Richard A. Loomis[b)]
Department of Chemistry, Washington University in St. Louis, Saint Louis, Missouri 63130

(Received 18 August 2006; accepted 20 September 2006; published online 25 October 2006)

The laser-induced fluorescence and action spectra of I_2 in a helium supersonic expansion have been recorded in the I_2 *B*–*X*, 20–0 region. Two features are identified within the spectra. The lower-energy feature arises from transitions between states that are localized in a T-shaped conformation on both the *X*- and *B*-state potentials. The higher-energy feature reflects transitions from states that are localized in a linear conformation on the *X* state to states that have energies that are larger than the barrier for free rotation of the rare gas atom about the I_2 molecule on the *B*-state potential. Ground-state binding energies of 16.6(6) and 16.3(6) cm^{-1} were determined for the T-shaped and linear conformers, respectively. These spectra are compared to those calculated using the experimentally determined rotational temperatures. Based on the agreement between the experimental and calculated spectra, the binding energies of the $J'=0$ states with 0 and 2–6 quanta of excitation in the He···I_2 bending mode on the *B* state were determined. Several models for the *B*-state potential were used to investigate the origins of the shape of the contour of the higher-energy feature in the spectra for He···I_2 and He···Br_2. The shape of the contours was found to be relatively insensitive to the choice of potential. This leads us to believe that the spectra of these systems are relatively insensitive to the parameters of the *B*-state potential energy surface and are more sensitive to properties of the halogen molecule. © *2006 American Institute of Physics*.
[DOI: 10.1063/1.2363378]

I. INTRODUCTION

Investigations of complexes of rare gas atoms M with halogen molecules XY have a long and rich history.[1–3] The relatively well-understood electronic structure of the halogen molecules, along with their strong optical spectra, makes them suitable for a broad range of experimental studies. The apparent simplicity of these triatomic systems has made them very attractive for comparisons of experiment and calculation, in particular, for testing various model potential surfaces.[3] In spite of this, new aspects of these systems emerge with each new set of experimental studies.

For example, until recently it was believed that the only transitions observed in the region of the *B*–*X* transition of XY originate from a conformer of M···XY in which the rovibrational wave functions on the *X* and *B* electronic states are localized in the minima near the T-shaped geometry of the complex.[4] Calculations showed that the angular range of the wave functions is narrow, even for the He···XY complexes, due to the rather small rotational constant for XY.[5] For example, in the case of He···Br_2, the width of the probability amplitude that corresponds to the lowest energy state in the T-shaped well on the *X*-state potential energy surface (PES) is approximately 30° (full width at half maximum).[6] The similarities between the *X*- and *B*-state potentials near the T-shaped minima make the assignment of the transitions originating from this conformer straightforward as the rare gas atom acts as a spectator, barely perturbing the rovibronic spectrum from that of the bare halogen molecule.

While high-level electronic structure calculations had predicted minima in the *X*-state potential in the linear He–X–Y configurations,[7] the experimental evidence of population in these wells was not definitively assigned until recently,[4,6,8,9] although they were first observed in the spectra of He···I_2 reported by Smalley *et al.* in 1976.[1] In the case of He···I_2, He···Br_2, and He···ICl, the depth of the linear and T-shaped minima are expected to be comparable.[6,7,10,11] The challenge in assigning the bands that originate from states that are localized near the linear minimum comes from the complicated structure of the band contour. In contrast to the band that results from transitions between states that are localized near the T-shaped minimum, the linear band does not have a structure similar to that of a single electronic transition of a diatomic molecule.

In earlier studies of the electronic spectrum of He···ICl (Ref. 9) and He···Br_2,[6] we showed that the structure of the linear band could be best described by transitions from states that are localized in the linear well on the *X*-state potential surface to a series of states on the *B*-state potential that can be best described as near-free rotor in character. Interestingly, while high-level *ab initio* electronic structure methods

[a)]Electronic mail: mccoy@chemistry.ohio-state.edu
[b)]Electronic mail: loomis@wustl.edu

were used to generate accurate representations of the *X*-state PES,[6,7,10,11] we found that we could reproduce the spectral envelope of the linear band when we employed pairwise-additive[12] or diatomics-in-molecules[13] (DIM) potentials to describe the *B*-state surfaces. We attributed the relative insensitivity of the contour of the linear feature in the spectrum to details of the *B*-state potential to the fact that the intermolecular vibrational states that are accessed in these transitions all lie above the barrier to free rotation of the rare gas atom about the dihalogen molecule.

In the present work, we focus on $He\cdots I_2$. As noted above, the linear feature in the spectrum was first reported by Smalley *et al.*, although at that time, they were not able to make a definitive assignment.[1] Using laser-induced fluorescence (LIF) and action spectroscopy approaches, we assign the features of the $He\cdots I_2$ spectrum and determine the binding energies of the $J=0$ states of all of the intermolecular levels on the $X(^1\Sigma_0^+)$ and $B(^3\Pi_0^+)$ state potentials that are involved in the transitions. The spectrum is calculated using a scaled version of the $He+I_2$ *X*-state potential of Prosmiti *et al.*[7] The scaling was introduced in order to reproduce the experimentally determined binding energies of the linear and T-shaped conformers. For the *B*-state PES, we employ three models. The most realistic of these is a pairwise-additive PES, based on the parameters for the $He\cdots I$ interactions of Waterland *et al.*[12] and a Rydberg-Klein-Rees (RKR) surface for I_2 of Barrow and Yee.[14] As with $He\cdots ICl$ and $He\cdots Br_2$, by introducing a scaling factor that is close to unity, we are able to reproduce the experimental band contours.

To investigate which properties of the *B*-state PES give rise to the observed spectra, two additional models are investigated. The first used the potential parameters that were previously developed to describe the *B*-state potential for $He\cdots Br_2$.[6,13] We also developed an elliptical surface in which the value of the potential energy depends only on the sum of the distances between the helium atom and the two focal points that are used to define an ellipse. Here, the positions of the focal points were chosen to ensure that the minimum energy separation at the linear and T-shaped geometries match those seen in the pairwise-additive *B*-state PES. In both cases, we obtained contours of the linear feature that were close to those observed experimentally. Further, these band contours were noticeably distinct from the shape of the corresponding contour for the $He\cdots Br_2$ spectrum.

This observation brings us back to one of the initial motivations of this series of studies. Specifically, the question of whether there is a simple explanation for the apparently complicated structure of the band contours of the linear features in these complexes. It seems that this feature is reflecting transitions from states that are localized in the linear well on the *X*-state PES to free rotor states on the *B*-state potential. As such, the most important properties for determining the contour of this band are the masses of the halogen atoms.

The remainder of the paper is organized as follows. In the next section we describe the experimental approaches taken in this study. This is followed by a brief discussion of the computational approaches. We then present the experimental and calculated binding energies of the states on the *X*- and *B*-state potentials that are probed experimentally. Finally, we discuss the sensitivity of these results to various parameters in our models.

II. EXPERIMENT

Ground-state, T-shaped and linear $He\cdots I_2(X,v''=0)$ van der Waals complexes were stabilized in a pulsed supersonic expansion by passing a pure helium carrier gas over room-temperature iodine crystals. The gaseous mixture with a total backing pressure in the range of 50–250 psi, relative to atmosphere, was pulsed at 10 Hz through either a 0.80 or 1.00 mm diameter orifice. LIF and action spectra were recorded at varying downstream distances in a manner previously described for $He\cdots ICl$.[15] Briefly, the LIF experiments were carried out with a Nd:YAG (yttrium aluminum garnet) pumped dye laser operating with rhodamine 575 or coumarin 152 dyes and a frequency bandwidth of 0.07(1) cm^{-1}. The laser beam was spatially filtered to a diameter of 2–3 mm, and pulse energies were <20 mJ inside the vacuum chamber. Resultant fluorescence in the expansion-laser interaction region was imaged, filtered to block laser scatter and pass fluorescence, and projected onto a photomultiplier tube (PMT).

Two-color action spectra were recorded by using the laser system described above and another Nd:YAG-pumped dye laser operating with coumarin 440 dye and a frequency bandwidth of 0.06(1) cm^{-1}. In these experiments, the pump laser was scanned through an I_2 $B-X$, $v'-0$ spectral region, with $v'=17-32$, exciting T-shaped or linear $He\cdots I_2(X,v''=0)$ conformers to metastable intermolecular vibrational levels lying within the $He+I_2(B,v')$ potential or I_2 monomers to long-lived $I_2(B,v')$ rovibrational levels, which fluoresce back down to the ground state. The probe laser was overlapped spatially with the pump beam and delayed 10–15 ns in time from the first. The wavelength of the probe laser was fixed on the rotational band head of an I_2 $E-B$, $v^\dagger-(v'-m')$ or I_2 $\beta-B$, $v^\dagger-(v'-m')$ transition, where $m'=0$ or 1. When probing the $v'-1$ channel, spectral features that are associated with transitions of the $He\cdots I_2$ complexes to excited-rovibrational levels within the $He+I_2(B,v')$ potential that would rapidly undergo vibrational predissociation forming $He+I_2(B,v'-1)$ products would be preferentially observed. Higher-order, $He_m\cdots I_2$ complexes, with $m\geqslant 2$, would undergo vibrational predissociation preferentially forming $mHe+I_2(B,v'-m)$ fragments when promoted to metastable, intermolecular vibrational levels within the $mHe+I_2(B,v')$ intermolecular potential, and thus intensities of features associated with transitions of higher-order complexes would be greatly reduced relative to those of the $He\cdots I_2$ complexes. An estimate of the relative intensities of these features was reported by Sharfin *et al.*[16] They reported that the ratio of products formed in the $2He+I_2(B,v'-1)$ relative to the $2He+I_2(B,v'-2)$ channel is 0.016 when exciting the T-shaped $He\cdots I_2(X,v''=0)$ complex to the lowest level within the $2He+I_2(B,v'=20)$ potential. Action spectra recorded with the probe laser fixed on a transition from an $I_2(B,v')$ level would detect transitions of I_2 molecules or

He···I_2 complexes that are prepared above the He $+I_2(B,v')$ dissociation limit and that undergo direct dissociation.[6,17–19]

Two-laser, pump-probe experiments aimed at accessing He···I_2 intermolecular vibrational levels associated with the He$+I_2(E\ 0_g^+, v^+=0,1)$ intermolecular potentials were performed using a similar experimental arrangement. The pump laser was fixed on a transition of either the T-shaped He···$I_2(X,v''=0)$ conformer to the lowest lying state within the He$+I_2(B,v'=23)$ potential, $n'=0$, also with a rigid T-shaped geometry, or the linear conformer to an intermolecular vibrationally excited level within the same B-state potential, $n'=3$, which is delocalized in the angular coordinate. The second probe laser is overlapped in time with the pump laser and is scanned in wavelength through the I_2 $E-B$, 0–23 or 1–23 regions to identify transitions of He···I_2 complexes to intermolecular vibrational levels lying within the He$+I_2(E\ 0_g^+, v^+=0,1)$ ion-pair state potentials. The fluorescence induced by the probe laser was filtered with a monochromator configured to pass specific I_2 $\beta \rightarrow A$ and $D' \rightarrow A'$ or $E \rightarrow B$ vibronic bands[20] with a spectral resolution of 7 nm.

III. THEORY

As in earlier work, the calculations of the spectra are performed in Jacobi coordinates (R,r,θ). Here, R represents the distance between the helium atom and the center of mass of I_2, r is the I_2 bond length, and θ is the angle between R and r. For the ground-state calculations we use the He $+I_2(X,v''=0)$ intermolecular PES reported by Prosmiti *et al.*[7] The potential was calculated for a fixed I–I distance of r_e $=2.666$ Å; the equilibrium bond length of I_2. The excited-state He$+I_2(B,v'=20)$ potential is described by the sum of the two He···I interactions $V_{\text{He–I}}$ and an I_2 potential V_{I_2},

$$V(r,R_i,\theta) = V_{\text{He–I}}(R_1) + V_{\text{He–I}}(R_2) + V_{I_2}(r), \tag{1}$$

where the $V_{\text{He–I}}(R_i)$ potentials are treated as Morse oscillators,

$$V_{\text{He–I}}(R_i) = D[(1-\exp[-\alpha(R_i-R_e)])^2 - 1], \tag{2}$$

and R_i represents the distance of the helium atom to one of the iodine atoms. We based this potential on the helium-iodine Morse interaction parameters from Waterland *et al.*, with $D=16.5$ cm^{-1}, $\alpha=1.5$ Å, and $R_e=4$ Å.[12] The I_2 potential used in this study is a spline interpolation of Barrow and Yee's RKR potential turning points.[14] The vibrational calculation is performed in two parts. First, we fix R and θ and calculate the energies for the I_2 vibrational states. These energies are used to generate the B-state adiabatic potential $V_B(R,\theta)$ for the intermolecular vibrational states probed experimentally.

The transition frequencies, intensities, and rovibronic spectra were obtained using previously described methods.[6,9] In short, the Hamiltonian for this system is

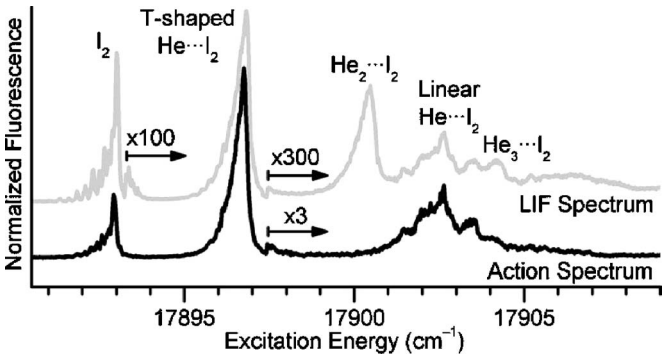

FIG. 1. Laser-induced fluorescence (LIF, gray) and action (black) spectra recorded in the I_2 $B-X$, 20–0 spectral region. The action spectrum was acquired with the probe laser fixed on the I_2 $\beta-B$, 0–19 rotational band head and is thus sensitive to detecting transitions of He···I_2 complexes in the 20–0 region and not those of higher-order complexes, observed in the LIF spectrum. The LIF spectrum is offset for clarity.

$$H = \frac{b}{\hbar^2}|\hat{\mathbf{J}}-\hat{\mathbf{l}}|^2 + \frac{\hat{\mathbf{l}}^2}{2\mu_R R^2} - \frac{\hbar^2}{2\mu_R}\frac{\partial^2}{\partial R^2} + V_{X,B}(R,\theta), \tag{3}$$

where $V_{X,B}(R,\theta)$ represents the potentials described above. The total angular momentum of the system is $\hat{\mathbf{J}}$, while $\hat{\mathbf{l}}$ is the angular momentum of the helium atom as it rotates around the I_2 center of mass. The Schrödinger equation is solved using a discrete variable representation (DVR) in R and θ. The DVR parameters are the same as those described for our work on He···Br_2.[6] A grid of 60 evenly spaced points in R, ranging from 2 to 10 Å is used, while the angular grid uses 30 DVR points based on the associated Legendre polynomials. While we have investigated several different levels of I_2 excitations, we focus on the surface generated when $v'=20$.

Once the energies and wave functions have been evaluated, we use this information to calculate the spectrum. As with He···Br_2 and He···ICl, we assume that the transition moment for I_2 is not perturbed by the presence of the helium atom. For $T \leqslant 1$ K, only states with $J'' \leqslant 9$ are significantly populated so only states with $J \leqslant 9$ on the X and B states were evaluated. For the calculations of the spectra, we account for the nuclear spin weightings in I_2, $\frac{7}{12}$ for states with odd parity and $\frac{5}{12}$ for states with even parity. The resulting stick spectra are convoluted with a Lorentzian function with a full width at half maximum of 0.12 cm^{-1} to facilitate comparison to experiment.

IV. RESULTS

A. Experimental results

Typical LIF and action spectra recorded in the I_2 $B-X$, 20–0 spectral region are plotted in Fig. 1 in gray and black, respectively. These spectra were recorded using a He-backing pressure of 250 psi and at 15.8 mm downstream along the expansion. The LIF spectrum contains a discrete feature associated with the I_2 monomer band at 17 893 cm^{-1}. Shifted nearly 4 cm^{-1} to higher energy is the previously observed feature associated with transitions of the states that are localized near the T-shaped minima of the He$+I_2(X,v''=0)$ potential to the lowest vibrational level on the He $+I_2(B,v'=20)$ potential.[1] Shifted by an additional 4 cm^{-1} is

a feature associated with transitions of the higher-order, $He_2\cdots I_2(X,v''=0)$ complex, which has both helium atoms localized in the T-shaped toroidal potential about the I–I bond axis.[21] To just higher energy than this feature is a series of lines that was observed previously but was not fully characterized.[1] Smalley *et al.* found that the intensity of this feature did not track with the intensities of the T-shaped $He\cdots I_2$ or higher-order $He_2\cdots I_2$ features as the He-backing pressure was systematically increased, thereby suggesting that a different species should be associated with this higher-energy feature.[1]

The action spectrum shown in Fig. 1 was acquired with identical expansion conditions as the LIF spectrum and with the probe laser fixed on the rotational band head of the I_2 β–B, 0–19 vibronic transition. In this manner, those spectral features associated with transitions of $He\cdots I_2(X,v''=0)$ complexes to rovibrational states within the $He+I_2(B,v'=20)$ potential can be identified, as contributions to the spectra from transitions of the I_2 monomer and higher-order $He_m\cdots I_2$ transitions are minimized. The T-shaped $He\cdots I_2$ feature at 17 897 cm^{-1} and the higher-energy feature at 17 903 cm^{-1} dominate the action spectrum. Note that there is negligible signal intensity associated with transitions of the higher-order $He_2\cdots I_2$ complex, which should be approximately 4 cm^{-1} higher in energy than the T-shaped feature. Based on the signal to noise of the spectrum, an upper limit of 0.01 can be placed on the ratio of forming the $2He+I_2(B,v'-1)$ product channel relative to the $2He+I_2(B,v'-2)$ channel. This value is only slightly lower than the ratio previously reported by Sharfin *et al.*[16] Based on similarities of these $He\cdots I_2$ spectra with published $He\cdots ICl$ (Refs. 9 and 22) and $He\cdots Br_2$ (Ref. 6) rovibronic spectra, we assign this higher-energy feature, centered near 17 903 cm^{-1} to transitions from the ground-state, linear $He\cdots I_2(X,v''=0)$ conformer to delocalized intermolecular rovibrational states within the excited-state, $He+I_2(B,v'=20)$ potential. The theoretical spectra presented in this manuscript provide strong support for this assignment.

In order to determine the relative stabilities of the linear and the T-shaped conformers, LIF and complimentary action spectra were recorded at varying downstream distances along the expansion. Similar experiments, performed on $He\cdots ICl$ (Refs. 22 and 23) and $He\cdots Br_2$,[6] revealed that with cooling along a He-carrier gas expansion, the relative populations of the T-shaped and linear conformers shifted to the energetically more stable species. Action spectra of $He\cdots I_2$, recorded with identical expansion conditions as those used to generate the action spectrum in Fig. 1, but at two different distances downstream, 8.9 and 70.7 mm, are seen in Fig. 2, plotted in black and gray, respectively. These spectra illustrate the observed changes in the intensities of the T-shaped and linear features. The $I_2(X,v''=0)$ rotational temperature at each distance was measured by fitting the rotational contour of the I_2 B–X, 20–0 monomer band in the LIF spectra which were recorded immediately following each action spectrum. Rotational temperatures of 1.86(2) and <0.09 K were measured for the two spectra plotted in Fig. 2. Since the linear feature at 17 903 cm^{-1} becomes less intense relative to the

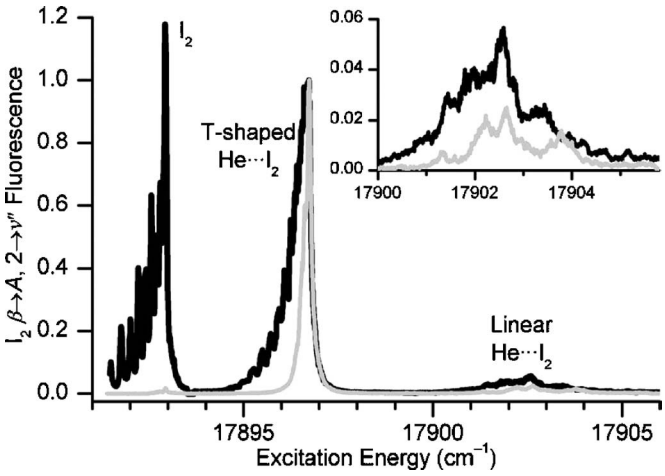

FIG. 2. Action spectra recorded in the I_2 B–X, 20–0 region with the probe laser fixed on the I_2 β–B, 0–19 rotational band head and at two different distances downstream along the expansion, 8.9 mm (black) and 70.7 mm (gray). The spectra are normalized to the peak intensity of the T-shaped $He\cdots I_2$ feature, and the inset is an expanded view of the region spanning the linear $He\cdots I_2$ feature.

T-shaped feature with cooling, the ground-state, linear $He\cdots I_2(X,v''=0)$ conformer is presumed to be less stable than the T-shaped conformer.

Action spectra were recorded with the probe laser fixed on the $\Delta v=0$ direct dissociation product channel to directly measure the binding energy of the ground-state, linear $He\cdots I_2(X,v''=0)$ conformer, in a similar manner as was reported previously when determining the binding energies of the linear $He\cdots ICl$,[15,17,22] $Ne\cdots ICl$,[19] and $He\cdots Br_2$ (Ref. 6) ground-state conformers. Action spectra were recorded in multiple I_2 B–X, $v'-0$ regions with the probe laser fixed on varying transitions from the $\Delta v=0$ direct dissociation product channels in the I_2 E–B, $v^{\dagger}-v'$ and I_2 β–B, $v^{\dagger}-v'$ regions. An action spectrum recorded in the I_2 B–X, 32–0 region with the probe laser fixed on the rotational band head of the I_2 β–B, 6–32 transition, with a backing pressure of 250 psi and at 11.9 mm downstream, is plotted in Fig. 3. A distinct onset of a continuum probe signal is observed approximately 16 cm^{-1} above the monomer band origin, presumably representing the threshold for bound-free transitions of $He\cdots I_2(X,v''=0)$ complexes. The intensity of this continuum signal was observed to track with the intensity of

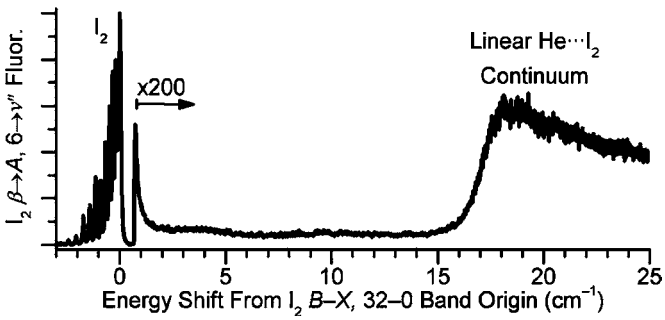

FIG. 3. Action spectrum recorded in the I_2 B–X, 32–0 spectral region and with the probe laser fixed on the band head of the I_2 β–B, 6–32 transition. The continuum signal at higher transition energies is found to track with the intensity of the linear $He\cdots I_2$ feature in the excitation spectra.

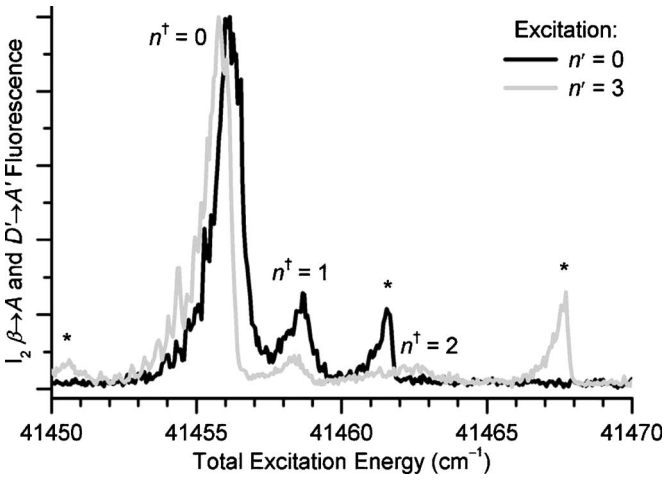

FIG. 4. Two-color, pump-probe spectra interrogating the intermolecular vibrational levels within the He+$I_2(E,v^\dagger=1)$ potential energy surface (PES). The pump laser was fixed on the T-shaped (18 159.3 cm^{-1}, black) and linear (18 165.4 cm^{-1}, gray) features in the I_2 $B-X$, 23–0 region, thereby accessing the $n'=0$ and 3 intermolecular vibrational levels within the He+$I_2(B,v'=23)$ PES, and the probe laser was scanned through the I_2 $E-B$, 1–23 region. Both spectra are plotted as a function of total photon energy, and fluorescence induced by the probe laser in the I_2 $\beta-A$ spectral region (338–345 nm) was collected using a monochromator. Asterisks denote features associated with transitions of bare I_2 molecules.

the linear feature and not the T-shaped feature in LIF and $\Delta v=-1$ action spectra recorded as the expansion conditions were varied. This suggests that the continuum is indeed attributable to transitions of the ground-state, linear He···$I_2(X,v''=0)$ conformer. Similar action spectra were recorded in the I_2 $B-X$, $v'-0$ regions with $v'=19$, 20, and 23. All of the action spectra contained continuum signals that are detected at the same transition energy above the corresponding monomer band origin and extending to higher energies. The average energies of the onsets of the continuum signals were used to set the binding energy of the ground-state, linear He···$I_2(X,v''=0)$ conformer at 16.3(6) cm^{-1}.

It was recently shown that the relative binding energies of the ground-sate, T-shaped and linear conformers of a rare gas-dihalogen complex can be directly measured by recording multiple, two-photon spectra and identifying spectral features associated with transitions to common intermolecular vibrational levels within the potential associated with the ion-pair state of the dihalogen.[24] The black spectrum in Fig. 4 was acquired with the pump laser fixed on the rotational band head of the T-shaped transition in the I_2 $B-X$, 23–0 spectral region, 18 159.3 cm^{-1}, thereby accessing the $n'=0$ level in the excited state and scanning the probe laser through the I_2 $E-B$, 1–23 region. In contrast, the gray spectrum was acquired in the same probe laser region with the excitation laser fixed on the linear feature in the 23–0 region, specifically to the $n'=3$ level with a transition energy of 18 165.4 cm^{-1}. Both spectra are plotted as functions of the total, pump-plus-probe, photon energy. Spectral features that can be attributed to transitions of I_2 molecules from the B state to low lying vibrational levels within the nested $E(0_g^+)$, $D(0_u^+)$, $\beta(1_g)$, and $D'(2_g)$ levels[20] are labeled with asterisks. The verification of the I_2 features was made by recording two-photon spectra in the same region but with the probe laser delayed by 30 ns from the pump. These spectra did not contain features associated with transitions from the short-lived He···$I_2(B,v'=23)$ levels, only those associated with transitions from the long-lived $I_2(B,v')$ levels.

TABLE I. Experimental energies of the He···I_2 conformers in the indicated vibronic states. The uncertainties are ±0.6 cm^{-1} dictated by the accuracy of the binding energy of the linear He···$I_2(X,v''=0)$ conformer.

Electronic state	Iodine vibrational level (v)	Intermolecular vibrational level (n)	Geometry	Energy (cm^{-1})
$X\,(^1\Sigma^+)$	0	0	T-shaped	−16.6
	0	1, 2	Linear	−16.3
$B\,(^3\Pi_0^+)$	19	0	T-shaped	−12.9
	20	0	T-shaped	−12.8
	21	0	T-shaped	−12.8
	22	0	T-shaped	−12.8
	23	0	T-shaped	−12.7
$E\,(0_g^+)$	1	0	T-shaped	−16.7

Somewhat surprisingly, the Franck-Condon factors for transitions from the two intermediate levels, the T-shaped and delocalized intermolecular vibrational levels in the He+$I_2(B,v'=23)$ potential, to levels in the ion-pair state are quite similar, with the lowest energy He···I_2 feature in each spectrum having the greatest intensity, as seen in Fig. 4. The relative intensity of the next feature to higher transition energy, at a total excitation energy of approximately 41 458.5 cm^{-1}, is more intense when using the T-shaped, $n'=0$ level as the intermediate. The next feature, at approximately 41 463.5 cm^{-1}, has slightly more intensity in the spectra recorded when exciting the delocalized, $n'=3$ level. Based on the same energy spacings between the He···I_2 features in the two spectra and the similar rotational contours of the features found at the corresponding transition energies, we conclude that the spectra access the same intermolecular vibrational levels within the ion-pair state potential. Specifically, we assign the features as transitions that access the three lowest intermolecular vibrational levels, $n^\dagger=0$, 1, and 2. The features observed in the two-photon spectrum acquired using the T-shaped, $n'=0$, excited-state level as the intermediate are observed to be 0.3(2) cm^{-1} higher in energy than those acquired using the $n'=3$ delocalized vibrational level as the intermediate. This difference is precisely the difference in the binding energies of the T-shaped and linear He···$I_2(X,v''=0)$ conformers, with the T-shaped conformer being more strongly bound.

From our determination of the linear He···$I_2(X,v''=0)$ binding energy of 16.3(6) cm^{-1}, we are able to set the binding energy of the T-shaped conformer to 16.6(6) cm^{-1}. The spectral shifts of the T-shaped features from the corresponding I_2 $B-X$, $v'-0$ monomer band origins indicate binding energies of 12.9(6)–12.7(6) within the He+$I_2(B,v')$ potentials, with $v'=19-23$. Specific values are listed in Table I. These values are just outside of the bracketed values of 13.6–14.8 cm^{-1} reported by Blazy *et al.*[25] The B-state binding energy and the spectral features recorded in the I_2 $E-B$, 1–23 region, seen in Fig. 4, enable us to set the binding

TABLE II. Energies of the lowest-energy, bound, intermolecular levels from the unscaled and scaled $He\cdots I_2(X,v''=0)$ potential. The experimental energies are −16.6(6) and −16.3(6) cm^{-1} for the T-shaped and linear complexes, respectively.

n''	$E^u_{n''}$ (cm^{-1})[a]	$E^s_{n''}$ (cm^{-1})[b]
0	−15.26	−16.59
1	−15.26	−16.33
2	−14.75	−16.33
3	−7.97	−8.97
4	−7.23	−8.04
5	−6.08	−7.03
6	−4.30	−5.24

[a]Unscaled potential.
[b]Potential multiplied by σ in Eq. (4).

energies of the three lowest levels, $n^{\dagger}=0$, 1, and 2, in the $He+I_2(E,v^{\dagger}=1)$ PES to 16.7(6), 14.1(6), and 10.7(6) cm^{-1}, respectively.

B. Calculated *X*-state vibrational wave functions and energies

The *X*-state potential is a two-dimensional slice through the three-dimensional PES of Prosmiti *et al.* at the equilibrium I–I bond distance, $r_e=2.666$ Å.[7] This potential $V_X(R,\theta)$ has a well depth at the linear orientation of $D''_e=43.52$ cm^{-1} at an internuclear distance of $R''_e=4.89$ Å. The values at the T-shaped orientation are $D''_e=37.32$ cm^{-1} with $R''_e=3.84$ Å.

We used this intermolecular potential to calculate energies and wave functions for $He\cdots I_2(X,v''=0)$ as described in the theory section above. The intermolecular energies for the bound states with $J''=0$ are presented in the second column of Table II. As in $He\cdots Br_2$,[6] the two lowest energy states are found to be localized in the potential well at the linear conformations of the complex, whereas the $n''=2$ state is localized in the well that corresponds to a 90° $He\cdots I_2$ angle, which we will refer to as the T-shaped well in the discussion that follows. This is not in agreement with the ordering of the experimental binding energies which has the T-shaped state more strongly bound than the ones that are localized near the linear well. To correct for this difference, we multiply the potential by

$$\sigma=[\alpha+\beta(1-0.5\cos^2(\theta))]. \quad (4)$$

Values of $\alpha=1.00$ and $\beta=0.08$ were chosen to match the experimental $J''=0$ energies for the lowest energy states on the *X*-state surface. This modification to the potential is analogous to the shifting of the *X*-state energies that we employed in our earlier study of the electronic spectrum of $He\cdots Br_2$,[6] and does not significantly affect the wave functions.

The scaled $He+I_2(X,v''=0)$ potential is plotted in Fig. 5(a) as a function of the Cartesian coordinates of the helium atom relative to the I–I center of mass, with the iodine atoms lying along the *x* axis. For the linear minimum, the potential has a well depth of $D''_e=45.24$ cm^{-1} at an internuclear distance of $R''_e=4.89$ Å. The potential values for the T-shaped minimum are $D''_e=40.00$ cm^{-1} with $R''_e=3.84$ Å. The $He\cdots I_2(X,v''=0)$ vibrational energies corresponding to this scaled surface are presented in the third column of Table II. Not surprisingly, this two parameter scaling of the PES provides energies that are in agreement with the two energies that are determined from the experiment.

What may, at first glance, seem surprising is the fact that the T-shaped conformer is more strongly bound than the linear one on the scaled surface, while the wells corresponding to the linear configurations of the complex still have a larger D''_e. This can be understood by comparing the values of the zero-point energy in the $He\cdots I_2$ stretch coordinate at the two geometries. To obtain these values, we look at a one-dimensional adiabatic picture of the potential; the details of which have been described elsewhere.[6] For the adiabatic calculations, the two-dimensional potential is averaged over the vibrational ground state in the $He\cdots I_2$ stretch for each point on the DVR grid in θ. When $\theta=0°$, the energy in the stretch coordinate is approximately 25 cm^{-1} while it is approximately 24 cm^{-1} at $\theta=90°$. Therefore, the difference in the zero-point energies compensates for the difference in the D''_e values at the two possible configurations.

The adiabatic potentials also serve to illustrate the localization of the wave functions. One might have expected that the wave functions for a complex of a helium atom with a dihalogen molecule would display very large amplitude zero-point motions. While this is certainly the case for the $He\cdots XY$ stretching motions, the amplitude of the angular

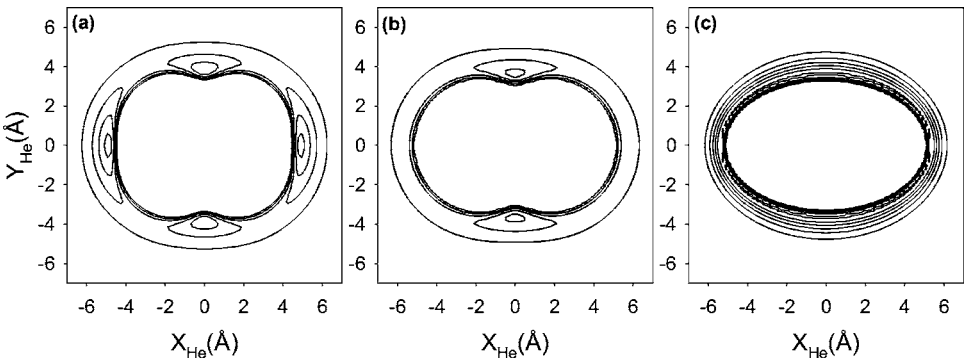

FIG. 5. The (a) $He+I_2(X,r=r_e)$, (b) $He+I_2(B,v'=20)$, and the (c) $He+I_2(B,v'=20)$ elliptical potential energy surfaces, described in the text. The potentials are plotted as functions of the Cartesian coordinates of the helium atom relative to the center of mass of I_2. The iodine atoms lie along the *x* axis. The highest energy contour is at +40 cm^{-1} and the contours are plotted in increments of 10 cm^{-1}. In all cases, the zero in energy corresponds to the dissociated $He+I_2$ products.

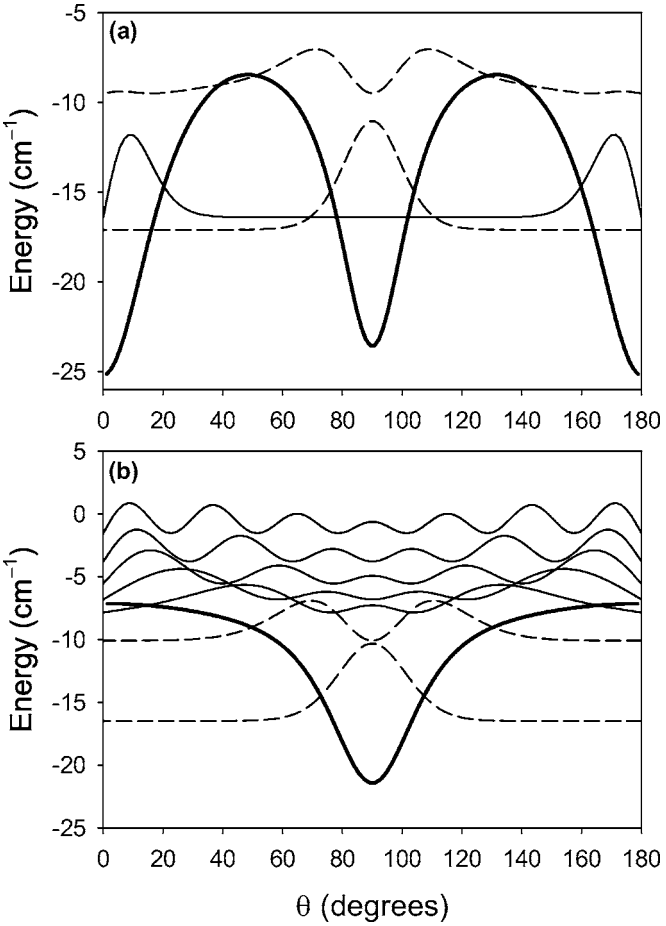

FIG. 6. The (a) He···$I_2(X,v''=0)$ and (b) He···$I_2(B,v'=20)$ adiabatic potentials (bold lines), plotted as functions of the He···I_2 angle θ with $\theta=0°$ and 180° corresponding to the linear He–I–I orientations. The probability amplitudes of the lowest-energy intermolecular vibrational eigenstates with $J=0$ are superimposed on the potentials. Each state is plotted so that zero amplitude corresponds to the energy of that state. Dashed lines indicate states that are localized in the T-shaped wells. Solid lines indicate states that are localized in the (a) linear wells and (b) free-rotor states.

motions is determined by the rotational constants for the XY molecule and for the He···XY complex. As both of these values are of the order of 0.01–0.1 cm^{-1} for He···I_2, the small effective mass leads to a much more localized behavior than one finds in, for example, complexes of Ar with HCl or HF.[26,27]

To illustrate the degree of localization of the wave functions that correspond to the energies in Table II, we plot their probability amplitudes superimposed on the adiabatic potential in Fig. 6(a). The probability amplitudes have been shifted so that zero probability corresponds to the energy of that state. The fact that the energies differ slightly from those reported in Table II is due to the introduction of the adiabatic separation of the He···I_2 stretching and bending motions. The plot shows that the lowest-energy state represents the helium atom being localized in a T-shaped configuration relative to the I–I bond. The next two lowest-energy states represent the symmetric and antisymmetric combinations of the two states that have the helium atom localized next to one of the two iodine atoms and near the I–I axis. Due to the small tunneling splitting between these two states, their probability amplitudes are indistinguishable in Fig. 6(a). These

TABLE III. Experimental energies as well as theoretical energies of the bound, intermolecular levels from the unscaled, scaled, and elliptical He $+I_2(B,v'=20)$ potential.

n'	Expt.	$E^u_{n'}$ (cm^{-1})[a]	$E^s_{n'}$ (cm^{-1})[b]	$E^e_{n'}$ (cm^{-1})[c]
0	−12.8	−13.54	−16.10	−11.14
1	···	−7.68	−9.46	−9.54
2	−7.9	−6.24	−7.65	−7.94
3	−6.8	−5.43	−6.75	−6.36
4	−5.7	−4.44	−5.80	−4.69
5	−4.2	−2.87	−4.24	−2.85
6	−2.2	−1.35	−2.67	−0.60

[a]Unscaled potential.
[b]Potential multiplied by 1.12.
[c]Elliptical potential.

three states are clearly localized within the bounds of the potential even though they differ in energy by <0.4 cm^{-1}. We therefore refer to the lowest-energy state, $n''=0$, as the T-shaped conformer and the next two lowest-energy states, $n''=1$, 2, as the linear conformers of He···$I_2(X,v''=0)$.

C. Experimental and calculated *B*-state binding energies

To obtain the *B*-state binding energies, we calculated the energies of the $v'=20$ state of I_2 as a function of R and θ using the pairwise-additive surface plotted in Fig. 5(b) and described in Sec. III. These energies are reported in the third column of Table III. Wave functions were also calculated and, along with the energies, were used to evaluate the energies and intensities of the rovibronic spectra for He···I_2 over the experimental rotational temperature range of 0.4–1 K.

The experimental *B*-state binding energy for $n'=0$ is easily obtained since the T-shaped feature results from transitions to this state. To assign the transitions responsible for the linear feature, we compared the calculated and experimental spectra in this region and found good qualitative agreement. This agreement could be improved if all the transitions which terminated at the same n' level in the calculated spectrum were shifted by a constant amount. The resulting experimentally derived vibrational band origins on the *B*-state surface are reported in the second column of Table III. To increase the agreement between the experimental and calculated energies, we multiply the *B*-state PES by 1.12. A similar scaling of 1.11 was previously applied to the *B*-state potential of the He···ICl complex.[9] We then recalculated our energies and wave functions using this scaled *B*-state potential, and the results are reported in the fourth column of Table III and in Fig. 6(b). Interestingly, as seen in Fig. 6(b), only the first two intermolecular states are localized in the T-shaped minimum. All other states are referred to as free-rotor states as the wave function has amplitude spreading over the full range of θ. For the remainder of our discussion, we will focus only on the scaled *X*- and *B*-state data.

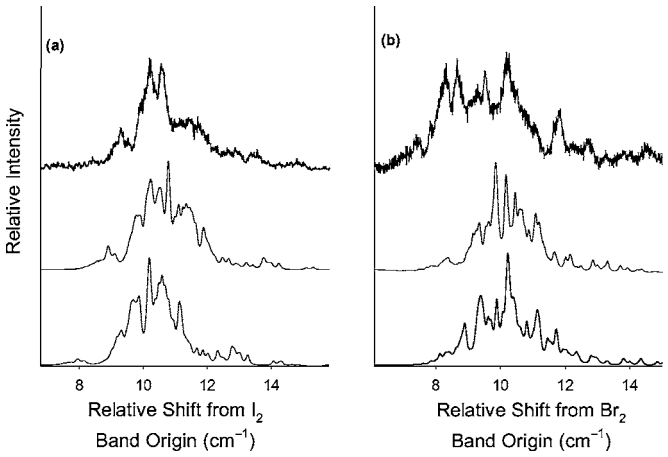

FIG. 7. The (a) experimental He···I_2 and the (b) experimental He···Br_2[6] spectra are plotted at the top with the corresponding spectra, calculated using the scaled PESs for the *X* and *B* state, plotted at the bottom. The center plots represent the He···I_2 spectrum calculated using the potential parameters of He···Br_2 and the He···Br_2 spectrum calculated using the potential parameters of He···I_2, as described in the text. All calculated spectra have a Lorentzian line width of 0.12 cm^{-1} and were calculated at 0.92 K. The two experimental spectra were recorded at (a) 0.92 K and (b) 0.91 K.

V. DISCUSSION

A. Comparison of the He···I_2 and He···Br_2 spectral features

One of the interesting findings from our series of studies on He···ICl, He···Br_2, and He···I_2 is the relative insensitivity of the shape of the spectral envelope to details of the *B*-state potential. As we have discussed previously,[6] this supports the fact that the T-shaped feature reflects a nearly vertical transition while the linear feature reflects transitions from states localized in the linear wells on the *X* state to free-rotor states, with $n'=2-6$, on the *B* state. However, the shape of the envelopes are found to be well described by a scaled pairwise-additive *B*-state PES for He···I_2 and He···ICl and a scaled DIM surface for He···Br_2. Since the spectra are well described by these simple models for the *B*-state potential, it is interesting that we are able to capture not only the structure of these seemingly complicated features but also the differences among them. The differences in the rotational contours of the He···I_2 and He···Br_2 linear features are shown in Figs. 7(a) and 7(b), where the top plot in each panel is the experimental spectrum and the bottom trace shows the corresponding calculated spectrum.

To investigate the origins of these differences, we performed two additional calculations of the spectra. For the middle trace of Fig. 7(a), we used the mass and rotational constants for I_2 with the *X*- and *B*-state potentials of He···Br_2. Likewise, for the spectrum in the middle of Fig. 7(b), we used the potentials for He···I_2 along with the mass and rotational constants for Br_2. Interestingly, the structure of the envelope of the spectra are relatively insensitive to the changes in the potentials leading us to believe that the differences between these spectra reflect the factor of 2 difference in the masses and the rotational constants for $Br_2(v'=12)$ and $I_2(v'=20)$.

B. Elliptical *B*-state potential and spectra

This simple picture of the dynamics is reassuring when we consider our past results for He···Br_2, where we found better agreement with experiment when we employed a DIM semiempirical *B*-state potential than when an *ab intio* potential was used.[6] To further extend this idea, we investigate a simpler model for the *B*-state potential. In particular, we describe the PES as an ellipsoid where the energy is a function of the sum of the distances of the helium atom from the two focal points that define an ellipse (r_1 and r_2),

$$V_{\mathrm{el}}(r_1,r_2)=D_e^{(\mathrm{el})}[1-\exp[-\gamma((r_1+r_2)-(r_e^{(\mathrm{el})}))]]^2-D_e^{(\mathrm{el})}, \tag{5}$$

where $D_e^{(\mathrm{el})}=31.05$ cm^{-1}, $r_e^{(\mathrm{el})}=4$ Å, and $\gamma=1.5$ $Å^{-1}$. The positions of the focal points and $r_e^{(\mathrm{el})}$ are chosen to ensure that the minimum energy He···I_2 separation at the T-shaped and linear configurations match those for our pairwise-additive *B*-state potential. The values of $D_e^{(\mathrm{el})}$ and γ are chosen to reproduce the $J'=0$ energies reported in the fourth column of Table III. In this model, we have removed the potential anisotropy, making the potential flat but elliptical in shape, to reflect the shape of the equipotential contours in the *B*-state PES of He···I_2. The resulting potential is plotted in Fig. 5(c).

Energies and wave functions were calculated for this elliptical potential, as described in Sec. III. The energies are reported in the fifth column of Table III. Rovibronic spectra were calculated and compared to the calculated He···I_2 spectra. While the spectra have noticeable differences due to the change of *B*-state potential, there are qualitative similarities within the linear feature. To highlight these similarities, we have plotted the stick spectrum of the linear bands from the rovibronic spectra calculated with the pairwise-additive *B*-state PES and the elliptical *B*-state PES in Figs. 8(a) and 8(b), respectively. The experimental He···I_2 spectrum is also plotted for comparison. Each line within the stick spectra is associated with a symbol that represents the excited-state intermolecular vibrational state accessed by that transition.

We have also calculated the analogous stick spectra using the DIM and elliptical *B*-state potentials along with the corresponding experimental spectrum for He···Br_2 in Figs. 8(c) and 8(d). Similar trends to those seen in He···I_2 are seen here. These trends further support our observation that the spectral envelope for the linear feature is more sensitive to the rotational constant and reduced mass of the halogen molecule than to features of the potential.

VI. CONCLUSIONS

Laser-induced fluorescence, action and two-laser, pump-probe spectroscopy experiments have been performed to determine the binding energies of He···I_2 van der Waals complexes associated with the ground X ($^1\Sigma_0^+$), valence B ($^3\Pi_0^+$), and ion-pair E (0_g^+) electronic states of I_2. Two distinct conformers are observed in the ground state: a T-shaped conformer bound by 16.6(6) cm^{-1} and a linear conformer bound by 16.3(6) cm^{-1}. Of the rare gas-dihalogen complexes for which both the T-shaped and linear conformers have been observed in rovibronic spectroscopy, this is the first system

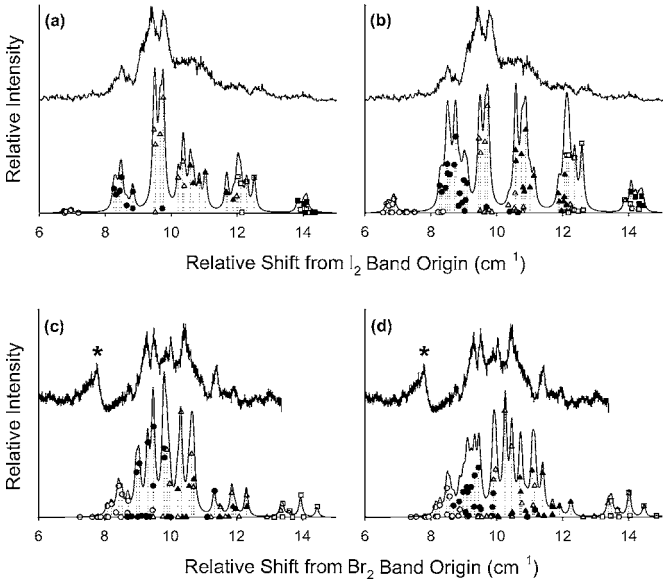

FIG. 8. Panels (a) and (b) show the calculated linear feature for $He\cdots I_2$ using the pairwise-additive *B*-state potential energy surface (PES) and the elliptical *B*-state PES, respectively. Panels (c) and (d) show the calculated linear feature for $He\cdots Br_2$ using the DIM *B*-state PES (Ref. 6) and the elliptical *B*-state PES, respectively. The corresponding experimental spectrum is the top plot in each of the four panels. The $He\cdots Br_2$ spectra have been published previously (Ref. 6), where the feature with the asterisk is a $He_2\cdots Br_2$ feature. The stick spectra associated with each panel have symbols representing the excited-state intermolecular vibrational levels accessed by each line: $n'=1$ (open circles), $n'=2$ (black circles), $n'=3$ (open triangles), $n'=4$ (black triangles), $n'=5$ (open squares), and $n'=6$ (black squares). These stick spectra have been shifted so that the band origins are at the experimentally determined values.

for which the T-shaped conformer is more strongly bound than the linear conformer. The $He\cdots I_2$ complexes in the *B* and *E* states are T shaped with binding energies of approximately 12.8(6) and 16.7(6) cm^{-1}, respectively.

Calculations of the $He\cdots I_2$ rovibronic spectra in the I_2 $B-X$, 20–0 region were performed using a scaled, high-level *ab initio* *X*-state potential[7] and a scaled, pairwise-additive *B*-state potential.[12,14] Comparisons of the calculated spectra to the experimental LIF and action spectra show good qualitative agreement. In particular, both spectra have intense features at low energy. These correspond to transitions between states that are localized in the T-shaped wells of the *X*- and *B*-state potentials. There is a second feature at higher energy that corresponds to transitions from states localized near the linear minima on the *X* state to free-rotor states on the *B*-state surface. These results are consistent with our findings for $He\cdots Br_2$.[6] However, when we compare the spectra of the two complexes, the contours of the T-shaped features are similar and resemble the monomer features, but there are noticeable differences in the contours of the higher-energy features.

These differences in the shape of the linear feature led us to examine their origins. We calculated spectra for $He\cdots I_2$ and $He\cdots Br_2$ using the potentials that were obtained for the other complex. Even with the change in potential, the spectra still showed good agreement with their experimental counterparts. These observations led us to believe the spectral structure is relatively insensitive to details of the *B*-state PES. Spectra calculated with an elliptical *B*-state potential are in qualitative agreement with experiment, further supporting this idea.

ACKNOWLEDGMENTS

Support through grants from the Chemistry Division of the National Science Foundation to two of the authors (A.B.M. and R.A.L.) is gratefully acknowledged. One of the author (R.A.L.) is indebted to the David and Lucile Packard Foundation for a Fellowship in Science and Engineering.

[1] R. E. Smalley, D. H. Levy, and L. Wharton, J. Chem. Phys. **64**, 3266 (1976).
[2] D. H. Levy, Adv. Chem. Phys. **47**, 323 (1981).
[3] A. Rohrbacher, J. Williams, and K. C. Janda, Phys. Chem. Chem. Phys. **1**, 5263 (1999).
[4] M. I. Hernandez, T. Gonzalez-Lezana, G. Delgado-Barrio, P. Villarreal, and A. A. Buchachenko, J. Chem. Phys. **113**, 4620 (2000).
[5] G. Delgado-Barrio, R. Prosmiti, A. Valdes, and P. Villarreal, Phys. Scr. **73**, C57 (2006).
[6] D. S. Boucher, D. B. Strasfeld, R. A. Loomis, J. M. Herbert, S. E. Ray, and A. B. McCoy, J. Chem. Phys. **123**, 104312 (2005).
[7] R. Prosmiti, A. Valdes, P. Villareal, and G. Delgado-Barrio, J. Phys. Chem. A **108**, 6065 (2004).
[8] A. A. Buchachenko, R. Prosmiti, C. Cunha, G. Delgado-Barrio, and P. Villarreal, J. Chem. Phys. **117**, 6117 (2002).
[9] A. B. McCoy, J. P. Darr, D. S. Boucher, P. R. Winter, M. D. Bradke, and R. A. Loomis, J. Chem. Phys. **120**, 2677 (2004).
[10] R. Prosmiti, C. Cunha, P. Villarreal, and G. Delgado-Barrio, J. Chem. Phys. **117**, 7017 (2002).
[11] A. Valdes, R. Prosmiti, P. Villareal, and G. Delgado-Barrio, Mol. Phys. **102**, 2277 (2004).
[12] R. L. Waterland, M. I. Lester, and N. Halberstadt, J. Chem. Phys. **92**, 4261 (1990).
[13] M. P. de Lara-Castells, A. A. Buchachenko, G. Delgado-Barrio, and P. Vilarreal, J. Chem. Phys. **120**, 2182 (2004).
[14] R. F. Barrow and K. K. Yee, J. Chem. Soc., Faraday Trans. 2 **69**, 684 (1973).
[15] J. P. Darr, R. A. Loomis, and A. B. McCoy, J. Chem. Phys. **122**, 044318 (2005).
[16] W. Sharfin, K. E. Johnson, L. Wharton, and D. H. Levy, J. Chem. Phys. **71**, 1292 (1979).
[17] J. P. Darr, A. C. Crowther, and R. A. Loomis, Chem. Phys. Lett. **378**, 359 (2003).
[18] J. P. Darr, J. J. Glennon, and R. A. Loomis, J. Chem. Phys. **122**, 131101 (2005).
[19] D. B. Strasfeld, J. P. Darr, and R. A. Loomis, Chem. Phys. Lett. **397**, 116 (2004).
[20] C. J. Fecko, M. A. Freedman, and T. A. Stephenson, J. Chem. Phys. **116**, 1361 (2002).
[21] J. E. Kenny, K. E. Johnson, W. Sharfin, and D. H. Levy, J. Chem. Phys. **72**, 1109 (1980).
[22] D. S. Boucher, J. P. Darr, M. D. Bradke, R. A. Loomis, and A. B. McCoy, Phys. Chem. Chem. Phys. **6**, 5275 (2004).
[23] D. S. Boucher, M. D. Bradke, J. P. Darr, and R. A. Loomis, J. Phys. Chem. A **107**, 6901 (2003).
[24] J. P. Darr and R. A. Loomis (unpublished).
[25] J. A. Blazy, B. M. DeKoven, T. D. Russell, and D. H. Levy, J. Chem. Phys. **72**, 2439 (1980).
[26] J. M. Hutson, J. Chem. Phys. **89**, 4550 (1988).
[27] J. M. Hutson, J. Chem. Phys. **96**, 6752 (1992).